

Experimental and simulation studies of resistivity in nanoscale copper films

A. Emre Yarimbiyik^{a,b}, Harry A. Schafft^b, Richard A. Allen^{b,*}, Mark D. Vaudin^c, Mona E. Zaghloul^a

^aThe Department of Electric and Computer Engineering, The George Washington University, Washington, DC 20052, United States

^bSemiconductor Electronics Division, National Institute of Standards and Technology, Gaithersburg, MD 20899-8120, United States

^cCeramics Division, National Institute of Standards and Technology, Gaithersburg, MD 20899-8520, United States

ARTICLE INFO

Article history:

Received 13 April 2007

Received in revised form 3 November 2008

Available online 24 December 2008

Keywords:

Copper
Interconnect
Matthiessen's rule
Resistivity
Size effects
Thin films

ABSTRACT

The effect of film thickness on the resistivity of thin, evaporated copper films (approximately 10–150 nm thick) was determined from sheet resistance, film thickness, and mean grain-size measurements by using four-point probe, profilometer, and electron backscatter diffraction (EBSD) and X-ray diffraction (XRD) methods, respectively. The resistivity of these films increased with decreasing film thickness in a manner that agreed well with the dependence given by a versatile simulation program, published earlier, using the measured values for the mean grain size and fitting parameters for surface and grain boundary scattering. Measurements of the change in sheet resistance with temperature of these films and the known change in resistivity with temperature for pure, bulk copper were used to calculate the thickness of these films electrically by using Matthiessen's rule (this is often referred to as an "electrical thickness"). These values agreed to within 3 nm of those obtained physically with the profilometer. Hence, Matthiessen's rule can continue to be used to measure the thickness of a copper film and, by inference, the cross-sectional area of a copper line for dimensions well below the mean free path of electrons in copper at room temperature (39 nm).

Published by Elsevier Ltd.

1. Introduction

The increase in the effective resistivity of copper interconnects as physical dimensions approach the bulk mean free path of electrons (approximately 39 nm at 25 °C [1]) is a serious concern because of the impact it has on reducing circuit speed. A model and a highly versatile simulation program, published earlier [2,3], were used to examine and predict size effects on the resistivity of thin metal films and lines [2,3]. The experimental effort reported here is intended to characterize the resistivity behavior of actual films and compare the results with the predictions of the previously introduced simulation program [3]. This program uses three input parameters. One is the experimentally determined mean grain size for a given film thickness. The other two are fitting parameters that characterize the scattering of electrons from the surfaces and from the grain boundaries within the film.

To a good approximation, metals such as aluminum and copper obey Matthiessen's rule [4], which states that the resistivity of a metal is equal to the sum of the temperature dependent resistivity of the pure, bulk form of the metal plus a tempera-

ture independent residual resistivity. This means that the change in resistivity with temperature of the metal is not affected by impurities or other sources of scattering that contribute to the increase in resistivity above that of the pure, bulk form of the metal. Hence, $(d\rho/dT)_{\text{pure,bulk}} = d\rho/dT$ of the metal as long as the metal obeys Matthiessen's rule. This is a powerful result because, with the value for $(d\rho/dT)_{\text{pure,bulk}}$, available in the literature [4], the thickness of a metal film and the cross-sectional area of a metal line can be calculated, respectively, from sheet resistance measurements of the film and from line resistance measurements made at two temperatures, respectively (the thickness of the films measured with this method will be regarded as "electrical thickness" throughout the paper). For films, $t = (d\rho/dT)_{\text{pure,bulk}} / (dR_s/dT)$, where R_s is the sheet resistance and t is the film thickness. It is therefore important to determine if and how Matthiessen's rule is impacted by size effects.

To obtain experimentally the dependence of copper resistivity on film thickness (size effect), copper films of varying thicknesses were evaporated on Pyrex and silicon wafers, and the sheet resistance and physical thickness of the films were measured. To look for a size effect on Matthiessen's rule, the change in sheet resistance with temperature, dR_s/dT , was measured for each film thickness. The value for $(d\rho/dT)_{\text{pure,bulk}}$ used in this paper is 0.0067 $\mu\Omega \text{ cm}/^\circ\text{C}$ [4].

* Corresponding author. Tel.: +1 301 975 5026; fax: +1 301 975 5668.
E-mail address: richard.allen@nist.gov (R.A. Allen).

2. Experimental

2.1. Deposition

A Denton Infinity 22¹ e-beam and resistance-heated evaporator² was used to deposit a very thin film of chromium (3 nm as indicated by the crystal sensor of the evaporator) and copper films from approximately 10 nm to 150 nm thick in order to study size effects on the effective resistivity of copper films. The wafers were nominally at room temperature during deposition. The chromium film serves to make the copper adhere to the Pyrex and Si wafers. Three-inch Pyrex wafers and 1-in. Si wafers were used as substrates. Films were deposited simultaneously on the two different types of substrate when the different measurements described below had contradictory requirements for the substrate. When the films were so deposited, the thicknesses of the films on the two substrates were assumed to be identical. In addition, a mask was used to provide a step for thickness measurements as described in Section 2.2. The manufacturer claims that the Pyrex wafers have a surface roughness of 1.5 nm. Copper pellets, 99.999% pure, were the source of the copper films. Chromium rods were used to deposit the chromium.

2.2. Thickness measurement

A Dektak profilometer was used to make physical thickness measurements of the film. There is approximately a 10 nm peak-to-peak noise in the output of the Dektak data, which may be partially caused by the surface roughness of the film. In order to obtain superior precision, the height levels were averaged over a distance of the scan on both sides of the transition using the Dektak software.

To be able to make a satisfactory measurement of the thickness of a film of copper with the Dektak profilometer required a well-defined, abrupt transition between the metal film and the substrate. This was obtained by the use of a special mask held in place by Kapton tape. Many mask materials were tried. By far the best was formed by breaking in two a thin ($\approx 170 \mu\text{m}$), 1 in. diameter (100) silicon wafer in such a manner that the fracture is along a (111) plane, which makes a 54.74° angle with the surface of the wafer and provides a knife edge at the bottom of the wafer (facing the Pyrex wafer). With such a sharp, straight edge in contact to the substrate, an abrupt edge to the copper film could be created.

2.3. Sheet resistance measurements

The sheet resistance is commonly measured by a four-point probe method (the four-point method is the preferred method of measuring sheet resistance, but is only applicable to non-patterned films; for patterned films, the Greek Cross variant of the van der Pauw structure provides optimal results). Four in-line, equally-spaced probes are placed in contact with the specimen surface and a current is passed between the two outer probes. The magnitude of this current is measured via the voltage across a standard resistor. The voltage is measured between the two inner probes. The current and voltage values are measured for forward and reverse current directions. The sheet resistance, R_s , is proportional to $R = V/I$, where V is the mean of the absolute values of the measured voltages. The proportionality factor is a function of the

geometry. For an infinite sheet with thickness much smaller than the probe spacing (which defines the samples measured in this paper), the sheet resistance is given by [5]

$$R_s = \frac{\pi V}{\ln 2 I} \quad (1)$$

This method has some important limitations, one of them being the necessity to locate the probes in high-symmetry positions in limited-area samples. To ensure that the measured R_s was not corrupted by Joule heating, the currents were scaled with the film thicknesses and select measurements were repeated at twice the current to ensure that R_s has not changed, which would indicate the presence of Joule heating.

A significant improvement for the four-point probe sheet resistance measurement is achieved with the dual configuration method [6], which makes it possible to make dependable sheet resistance measurements quite close to the rim of the wafer or near any area in the wafer clear of copper. In this method, measurements with the traditional configuration, explained above, are made. Then, current is conducted between one outer and the more distant inner probe, while the voltage is measured across the remaining two probes. In this second configuration, the voltage and current values in the forward and reverse directions are measured. The scaling factor K is determined from a transcendental equation [6]. A highly accurate value for this K factor can be obtained [6] using the following quadratic fit:

$$K = -14.696 + 25.173 \left(\frac{R_1}{R_2} \right) - 7.872 \left(\frac{R_1}{R_2} \right)^2 \quad (2)$$

where R_1 and R_2 are the voltage-to-current ratios in the first and second electrical configurations, respectively. This simplification is valid if the value for R_1/R_2 is within the interval [1.18, 1.3] [6]. Values obtained for this ratio were usually 1.24. The sheet resistance in the dual configuration method is

$$R_s = KR_1 \quad (3)$$

The standard deviation of sheet resistance measurements made by use of the dual configuration method was at most 0.3%, when repeated measurements were made by raising the probe head between measurements. An in-house built measurement system³ and probe heads⁴ were used to make the sheet resistance measurements.

2.3.1. Location of thickness and sheet resistance measurements to calculate resistivity

A mask, as described in Section 2.2, was placed close to the rim of each Pyrex substrate. Hence, the physical measurement of film thickness with the profilometer was made away from the center of the wafer. This was done so that a large area of the copper film in the central part of the wafer would be available for the four-point probe measurement of sheet resistance. The resistivity was calculated from the sheet resistance measurement near the center of the wafer and the value of the physical thickness obtained from measurements near the rim of the wafer. This could be done because previous measurements of the sheet resistance along the diameter of wafers consistently indicated that the film thickness was constant over the wafer. That this is, in fact, true is substantiated by the observation (shown later in Fig. 5) that the physical

¹ Certain commercial equipment, instruments, or materials are identified in this paper in order to specify the experimental procedure adequately. Such identification is not intended to imply recommendation or endorsement by the National Institute of Standards and Technology, nor is it intended to imply that the materials or equipment identified are necessarily the best available for the purpose.

² This work was performed in part at the NIST Center for Nanoscale Science and Technology's Nanofab facility in Gaithersburg, MD.

³ The electronics and the probe heads in this system meet, or exceed, all performance aspects of ASTM Method F-84 for measurement of bulk silicon resistivity by four-point probe, and ASTM Method F-374 for measurement of sheet resistance of thin conducting films on silicon wafers. This system has been used for a number of years to certify silicon resistivity standards (NIST Standard Reference Materials) that are used world-wide in industry, academia, government labs, and other national standards laboratories.

⁴ The separation of the probes in the probe head used is 0.635 mm (25 mils).

thickness measured near the rim of the wafer (with the Dektak) and the electrical thickness measured near the center of the wafer using Matthiessen's rule agreed within 3 nm.

2.3.2. Measurement of dR_S/dT

To learn the thickness below which Matthiessen's rule can no longer be used to make an accurate measurement of film thickness, we made measurements of the sheet resistances of each film near the center of the wafer at three temperatures over a range of approximately 61 °C to obtain a value for dR_S/dT . For these films, the forcing currents ranged from 5 mA for the 10-nm film to 25 mA for the 150-nm film. It was necessary to make the measurements near the center because when such sheet resistance measurements were made near the edge of a region uncovered with metal (within a centimeter), large over-estimates of the thickness were obtained. The reason for this edge effect in the use of Matthiessen's rule to measure thickness is not known.

To determine the value of dR_S/dT for a film of a given thickness, the sheet resistance was measured at approximately 28 °C, 60 °C, and 89 °C, in that order. To assure that the film was not oxidized or otherwise changed by the temperature excursion, the sheet resistance of the film was measured again at 28 °C. Values for dR_S/dT are entered in Table 1 only if the initial and final measurements of the sheet resistance agreed to within the precision of the sheet resistance measurements. A high degree of linearity was indicated by values for the coefficient of simple determination, r^2 [7], which were all greater than 0.995. With the experimentally determined value for dR_S/dT and change in the resistivity with temperature of pure, bulk copper [4], it is possible to determine the electrical film thickness using Matthiessen's rule from $(d\rho/dT)_{\text{pure,bulk}}/(dR_S/dT)$.

2.4. Grain size measurements – introduction

The resistivity calculated by the simulation program depends strongly on the parameters of the material that impact the transport of the conduction electrons. A key parameter for the simulation program is the mean grain size in the plane of the film. To obtain values for this parameter, three methods were used. The first was atomic force microscopy (AFM). The topography measured using AFM did not scale with the thickness of the copper films, as would be expected if it were indicative of the underlying grain structure. In fact, the peaks and valleys observed in the AFM images, an example of which is shown in Fig. 1, were of the order of 20 nm irrespective of film thickness.

To determine the mean grain size in all of the films required the combined use of the X-ray diffraction (XRD) and the electron back-scattered diffraction (EBSD) methods. Each method is discussed in more detail below. EBSD [8,9] is a scanning electron microscopy (SEM)-based method of identifying the grain orientation at any point on the surface and can be used to map the grains in the plane of the film. An immediate result from the EBSD measurements was

that most of the topography visible in AFM (and for that matter, SEM) images is generally not correlated to the actual size of the grains. Another result was that the spatial resolution limitations of the method permitted an analysis of images obtained for only the two thickest films. On the other hand, the XRD method was able to provide mean grain size values for all film thicknesses. But, this method provides only a measure of the grain size normal to the surface of the film (thickness) [10]. The experimentally determined relationship between the mean grain sizes obtained from the two methods for the two thickest films suggested the use of a scaling factor that led to size values that could be used by the simulation program.

2.4.1. Average grain size measurement using X-ray diffraction

In XRD, the sample is placed such that an X-ray beam strikes the surface of the wafer and diffracts from the film deposited on it. The diffraction pattern is analyzed to give information about the crystal structure and microstructure of the copper film. The diffractometer used in this study was a Siemens D500 equipped with a Ge monochromator tuned to pass only the $\text{CuK}_{\alpha 1}$ wavelength and not $\text{CuK}_{\alpha 2}$, resulting in narrower Bragg peaks which are easier to analyze for broadening and give more accurate results.

Intensity vs. scattering angle plots are obtained from XRD measurements and used to calculate a grain size with Scherrer's equation (1918) [11]:

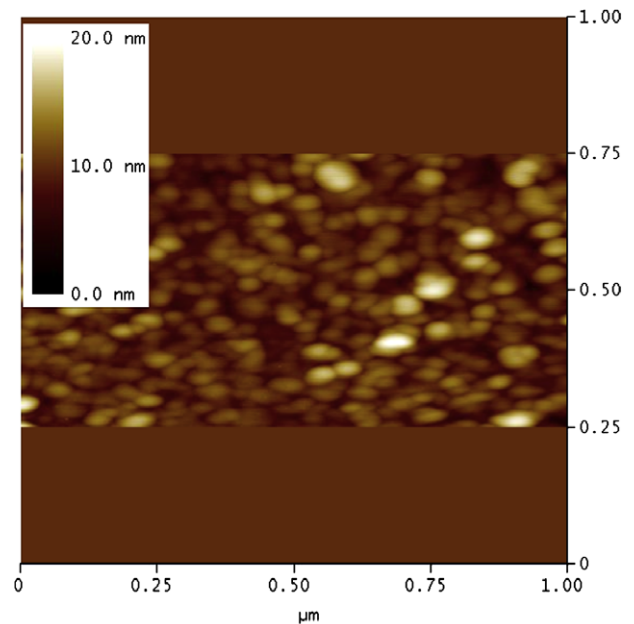


Fig. 1. AFM image of the surface of the nominally 100 nm thick film.

Table 1

Measurements of thin, copper films evaporated on Pyrex wafers. Listed are data for thickness measurements (Dektak), corrected for oxidation (except for the 150 nm film) and for the Chromium adhesion layer; data for sheet resistance and dR_S/dT ; and calculations of film thickness using Matthiessen's rule.

Target thickness (nm)	Corrected thickness (Dektak) (nm)	Sheet resistance normalized to 28.6 °C (Ω/\square)	dR_S/dT ($\Omega \times 10^{-6}/\text{°C}$)	Thickness calculated with Matthiessen's rule (nm)
10	9.2 ± 3.6	13.928 ± 0.02	9673	6.9
20	21.1 ± 2.6	3.652 ± 0.003	3369	19.9
30	34 ± 3.6	1.612 ± 0.002	2047	32.7
40	42.2 ± 3.1	1.137 ± 0.002	1568	42.7
50	50.7 ± 4.1	0.8839 ± 0.0003	1347	49.8
70	70.1 ± 7.1	0.5538 ± 0.0006	957	70
100	111 ± 2	0.29676 ± 0.00005	599	111.85
150	166.1 ± 2.6	0.17958 ± 0.00016	409	163.93

$$D = K\lambda/\beta \cos \theta \quad (4)$$

where D is a measure of the grain dimension, λ is the wavelength, β is the pure diffraction broadening, and θ is the Bragg angle of the hkl peak. K is a constant that depends on crystallite shape, the hkl Miller indices, and the definitions taken for β and D . Values for K can range from 0.7 to 1.7. When β is taken as the half-maximum intensity line breadth and D is defined as the mean dimension of the grain perpendicular to the diffracting planes, K is shown to have a value of about 0.9 [12], which is the value in the software package that is used to analyze the XRD data. This definition of D is used, because the crystallite shape is unknown and may vary from crystal to crystal [10]. Instrumental contribution to the broadening needs to be taken into account; it was determined to be 0.15° . Various corrections can be made based on different assumptions about the summation of the instrument and specimen profiles: simple summation (Lorentzian profiles), summation in quadrature (Gaussian profiles), and a mixed summation (Lorentzian/Gaussian) [13]. Gaussian profiles are assumed throughout this paper. The instrumental broadening of 0.15° has the largest relative effect on narrow experimentally observed peaks which correlate with larger grain sizes. In our experiments, experimental peak widths from 0.2° to 0.8° were observed.

Applying the definitions above for β and D , the XRD method provides the mean thickness of the grains in the z direction, GS_z , which is perpendicular to the plane of the thin film. However, our interest is in the mean size of the grains in the xy plane, GS_{xy} , because it is the effective dimension used in the simulation program and calculation. GS_{xy} is the mean value of the equivalent circle diameters (ECD) [14] of the grains in the xy plane.

Because the GS_z calculation is dependent on the K constant, the results should not be regarded as an absolute measure of the grain size in the z direction unless the correct K value is known. This is not the case for the measurements reported in this paper; however, GS_z measurements in films with different thicknesses can be used if we can assume that the mean size of the grains in the x - y plane is proportional to the size of the grains (in the z direction).

2.4.2. Grain size measurement using electron backscattered diffraction

EBSD [8,9] is a SEM-based tool for evaluating the crystal structure of a crystalline or polycrystalline material. It uses a scanning electron microscope which has been equipped with a special backscatter detector which provides spatial information on the direction backscattered electrons take after leaving the surface of the material, which has been placed in the scanning electron microscope at an angle of between 60° and 70° (in this work, an angle of 68° was used). This detector is typically a phosphor-coated screen; electrons hitting the surface fluoresce the screen and the light is captured creating a diffraction pattern. The EBSD system used in this study is manufactured by Oxford Instruments HKL.

Note that in a conventional scanning electron microscope, the backscatter detector is located above the sample and does not collect information on where the electrons hit the detector. This type of backscatter detector counts the number of electrons that impinge on the detector and assigns a grayscale value based on this count. This image is most useful when looking at mixed phase materials, where grains of different average compositions produce different contrast.

In EBSD, the interactions of the electron beam with the planes of atoms that make up the surface of the material imaged that satisfy Bragg conditions create bright bands, called “Kikuchi bands” on the fluorescent screen. The unique pattern of the Kikuchi bands is characteristic of both the crystal structure and orientation in the region sampled. The band contrast (BC), or intensity, and band slope (BS), or sharpness, are strongly affected by the perfection of the crystal-

line region that is diffracting. High dislocation densities and very small grain sizes (in our case approximately 10 nm) both lead to patterns with weak (low BC), fuzzy (low BS) bands.

The EBSD system is equipped with software tools that have been developed to reveal the grain morphology and crystalline orientation of a known material. Further, an x - y map revealing the grain microstructure can be made under automatic computer control by collecting and analyzing a diffraction pattern over a rectangular grid of locations. At each pixel in the map, a pattern is obtained. The positions of the most intense Kikuchi bands in the pattern are determined, and, from this information, the angles between the diffracting planes that produced the bands are calculated. This set of angles is compared with a calculated set of angles between planes in the crystal structure of the material being analyzed, in this case fcc copper. Each subset of angles being compared with the experimental angles corresponds to a specific indexing of the pattern and also a specific orientation of the diffracting crystal. The mean angular deviation (MAD) for each trial indexing scheme is the average angular difference between the experimentally determined and crystallographically calculated interplanar angles. The indexing with the smallest MAD is selected to give the crystal orientation at that pixel in the map. The analysis process is automated so that many orientations per second can be determined. The maximum allowable MAD is set by the user and was set at 2° for the majority of the scans. As in all SEM imaging modes and in contrast with the XRD described above, EBSD provides an “image” of the grain structure of the near-surface region of the feature being measured.

As discussed in Section 2.4, the experiment reported in this paper combines the independent tools of EBSD and XRD to evaluate the grain sizes of copper films with a number of different film thicknesses. EBSD and XRD measurements were taken on the films deposited on 1-in. Si wafers because (1) Pyrex substrates are poor conductors and charge in the scanning electron microscope and (2) 3-in. wafers are too large to fit in the scanning electron microscope and in the X-ray diffractometer. Three-inch Pyrex wafers with masks were included in this second set of depositions to measure the physical thickness of each deposition to obtain grain size vs. thickness data. (In the first deposition, three-inch Pyrex wafers were used. These wafers were used for the sheet resistance vs. thickness measurements as well as the physical vs. electrical thickness comparison. A second set of depositions were performed simultaneously on 1-in. Si and 3-in. Pyrex substrate wafers, so that the grain size vs. thickness could be measured. Grain sizes were measured on the silicon wafers while physical thicknesses were measured on the Pyrex wafers.)

3. Measurement results and discussion

Results of sheet resistance measurements taken from the 3-in. Pyrex wafers over a range of temperatures, thickness measurements, and calculations are listed in Table 1. Columns 1 and 2 of the Table 1 list, respectively, the target film thicknesses and the values for the film thickness as measured by the Dektak profilometer. Repeated thickness measurements with the profilometer showed a mean standard deviation of 3.6 nm. All of these thickness values have been corrected for the 3-nm thick chromium film. Although the samples were kept in a nitrogen box, except for transport or measurements, oxidation effects had to be taken into account in the thickness measurements, because of the long storage time between film deposition and the sheet resistance measurement. Therefore, all but the value for the 150 nm film were also corrected for a reduction of film thickness caused by oxidation. This correction is discussed in the following paragraph. Column 3 lists the measured values for the sheet resistance, normalized to

28.6 °C (range: 28.1–29.0 °C). The resistivity of each film thickness is obtained from the product of the thickness in column 2 and the sheet resistance in column 3. Column 4 lists the change in sheet resistance with temperature over a range from approximately 28 °C to 90 °C for all film thicknesses. The re-measured sheet resistance at 28 °C did not show any change from its initial value, indicating that there was little or no oxidation of the sample due to the temperature excursions. The inverse of each of these values multiplied by the change in resistivity with temperature of pure, bulk copper ($0.0067 \mu\Omega \text{ cm}/^\circ\text{C}$ [4]) provides an electrical measurement of the film thickness based on the use of Matthiessen's rule.

The correction for copper consumption due to oxidation that was used to arrive at the values listed in column 2 of Table 1

Table 2

List of grain thicknesses, GS_z , and grain sizes in the film plane, GS_{xy} , calculated with the assumption that GS_z is directly proportional to GS_{xy} .

Target thickness (nm)	Dektak Thickness (nm) (with a standard deviation of ± 2.5)	GS_z (nm)	GS_{xy} (nm)
10	10	8	5
20	24.7	17	10
40	40.4	23	13
70	69	39	22
100	96.6	51	30
150	149.9	69	40*

The symbol "*" denotes that the value for the proportionality constant, GS_{xy}/GS_z , obtained from the nominal 150 nm film was used to calculate the value of GS_z for the other films.

was determined as follows. Matthiessen's-rule calculations for the nominal 30 nm and 40 nm thick films, which were made 14 days after deposition, yielded calculated thickness values of 38.8 nm and 49.1 nm, respectively. When these thickness measurements were repeated over 100 days later, shortly before sheet resistance measurements were made, calculated thicknesses values of 32.7 nm and 42.7 nm were obtained. These calculations are reliable because there is high degree of linearity ($r^2 = 0.999999$ and $r^2 = 0.999953$, respectively) in each of the dR_s/dT plots. Assuming that the oxidation formation is independent of the film thickness, it was concluded that an average of 6.25 nm of copper had been consumed by the oxidation that had occurred for all but the nominal 150 nm film, where the sheet resistance measurements were measured only 33 days after the thickness of the film was measured. The correction for this film (were it to be used) would be somewhat less than 6.25 nm.

The EBSD measurement performed for the 100 nm thick film yielded a grain size of 33 nm. Within experimental error, this value is equal to the value (30 nm) shown in column 4 of Table 2. Note that only those collection of pixels greater than or equal to 6 in number are counted as grains, and the pixels are 8 nm on a side, so that the minimum grain size that can be measured with this electron beam step size is 11 nm. The mean grain size measurements made on the 1-in. Si wafers are summarized in Table 2. The first two columns in Table 2 list the target and measured copper-film thicknesses (10–150 nm). The values for GS_z determined from XRD measurements of these films are given in the third column. Column 4 is obtained with the assumption that the grain size

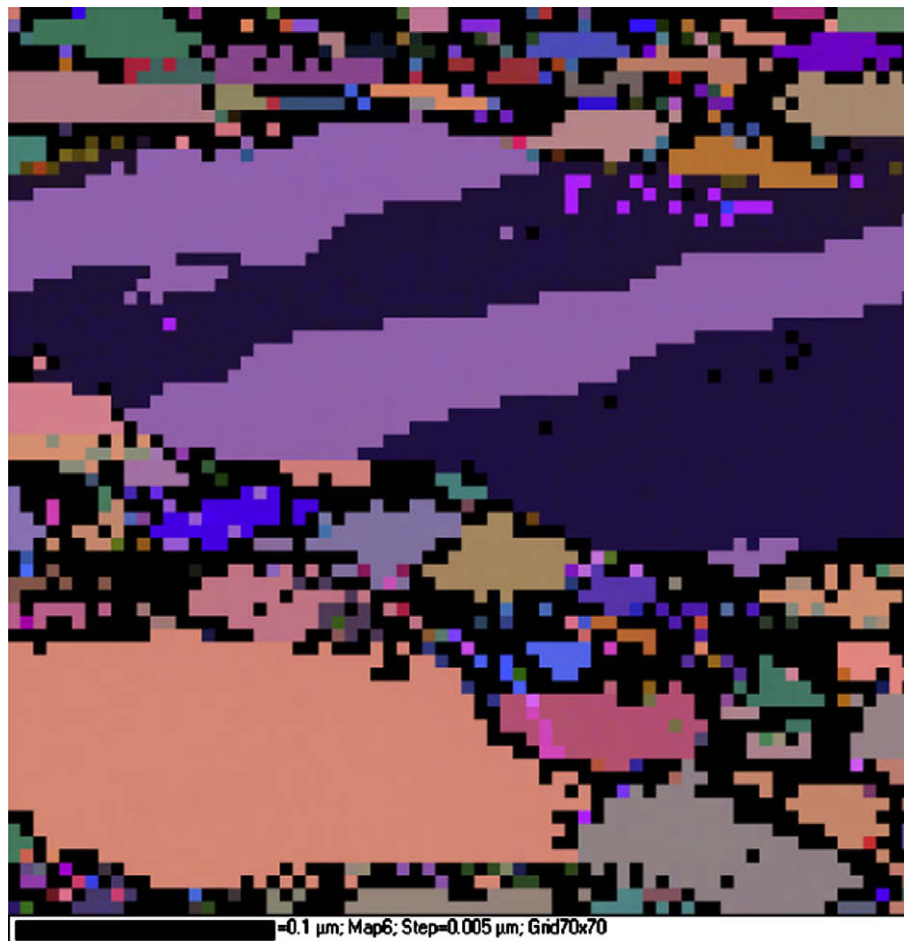


Fig. 2. EBSD image for the 150 nm film. There are a few large grains with twins and numerous small grains. Average grain size is 40 nm.

in the xy plane is directly proportional to the grain size in the z direction; i.e. the average aspect ratio of the grains in the film was constant. The proportionality constant $GS_{xy}/GS_z = 0.58$, obtained using the data for the 150 nm film, was used to obtain GS_{xy} values for the other films in column 4. The image of the grain structure obtained with the EBSD technique of the 150-nm film is shown in Fig. 2 (note that each pixel in Fig. 2 covers a square, 5 nm on a side.). The data shown in Fig. 2 were used to obtain a value for the mean grain size in the xy plane of the 150-nm film, namely, GS_{xy} (150 nm). A grain was considered to exist if ten or more pixels of the same color were connected (in the case of twins, such as seen in Fig. 2, each is treated as a separate grain). The size of each grain was characterized by the diameter of a circle that has the same area as that calculated for the grain. GS_{xy} (150 nm) is equal to the mean of all of the equivalent circle diameters (ECD) [14]. From this result, and the assumption described above, the mean grain size as a function of film thickness for the remaining films are calculated; these grain sizes are plotted in Fig. 3 where a nearly linear dependence is shown ($r^2 = 0.988$).

The EBSD measurement performed for the 100 nm thick film yielded a grain size of 33 nm (only the collection of pixels that are more than or equal to six are counted as grains, where the step size is 8 nm on a side). This value is within approximately 3 nm of the value (30 nm) shown in column 4 of Table 2. This result lends validity to the proposition that grain size in the xy plane is directly proportional to the grain size in the z direction. In all, 15 EBSD maps were collected from all the films deposited on Si. Only the 150 nm and 100 nm films (shown in the first two rows of Table 3) produced maps of sufficient quality to allow grain sizes to be determined. Thus the relationship between grain size in the xy

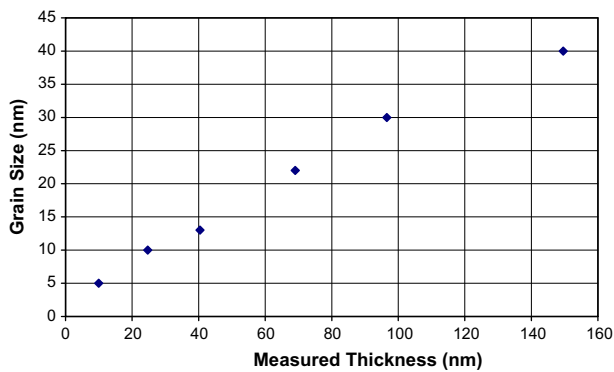


Fig. 3. Mean grain size (GS_{xy}) vs. thickness plot for the data in Table 2.

plane and grain size in the z direction could not be confirmed with data at smaller film thicknesses.

Table 3 shows EBSD data for all 14 maps. The following data are given: the average BC and BS numbers for pixels indexed as Cu and for pixels where indexing was not possible (the so-called zero solutions); hit rate (fraction of pixels where an orientation determination was made); and MAD. The thinner films produced diffraction patterns which on average had lower values for BC and BS. This resulted in maps in which either a relatively small hit rate was achieved, or else the orientation determined at a large fraction of pixels was incorrect, which could be determined by inspection (if very few or none of the eight adjacent pixels had similar orientations assigned to them). For a number of maps, the Cu and zero solutions have very similar BC and BS values, and the hit rate is relatively high ($\approx 65\%$), showing that much of the indexing was spurious and most likely due to an injudicious choice of indexing parameters. It is suggested that the films (as grown) have a high dislocation density and very small grain size, resulting in the poor quality of the diffraction patterns observed in the thinner films (<100 nm). It is noticeable in Fig. 2 that the grain size distribution is bimodal with most grains being in the 30–50-nm range as well as a smaller number of grains being larger than 100 nm. The smaller grains had BS values averaging around 150, while almost all the pixels in the larger grains had the maximum possible BS value of 255 (i.e., very high quality diffraction patterns). This is consistent with recrystallization having occurred in all the grains in the film, with the most extensive recrystallization occurring in the largest grains. The thinner films (<100 nm) all had average BS values less than 100 and, thus, appear to have undergone less extensive recrystallization. In EBSD observations of microstructure evolution in thermally-cycled Al interconnects, Keller et al. [15] have observed that, when a grain is growing and consuming its neighbor, the pattern quality for growing grains was greater than that of the consumed grains. Texture measurements on the films using XRD show that there is significant $\{111\}$ texture in the films with the thickest films having the greatest degree of texture. This again is consistent with the thicker films having recrystallized the most with recrystallization favoring creation of $\{111\}$ oriented grains.

The effect of film thickness on the resistivity of evaporated copper films is shown in Fig. 4, where the resistivity is calculated from the data in columns 2 and 3 in Table 1. One-standard-deviation confidence limits are shown and are essentially the same for resistivity and for thickness because the standard deviations for thickness measurements, generally 3 nm to 4 nm, are so much larger than those for sheet resistance measurements ($<0.3\%$).

Also shown in Fig. 4 are data points determined from using the simulation program [2] with the dependence of grain size, GS_{xy} , on

Table 3
Data from 14 EBSD maps obtained from 4 films. Data sorted in order of BS copper (column 3). Top 2 data sets used in analysis.

Film thickness (nm)	Copper solutions		Zero solutions		Hit rate (%)	MAD ^o
	BC	BS	BC	BS		
150	76.14	216.7	38.23	138.2	77.08	0.7318
100	48.85	161.4	21.42	110.1	47.97	0.8563
150	58.02	144.8	39.24	122.7	45.92	0.9328
100	40.95	135.2	24.63	104.4	39.43	0.9223
100	53.57	120	32.47	105.7	25.34	1.008
100	27.99	114.1	16.25	104.2	17.16	1.249
70	29.49	98.69	22.82	97.07	75.51	1.014
70	29.6	98.1	22.9	97.17	19.85	1.149
70	33.62	98.04	27.63	93.48	69.86	1.021
70	23.95	95.74	22.41	96.37	66.15	1.118
100	23.6	93.8	23.63	90.04	8.40	1.115
70	90.07	89.91	22.68	23.07	60.77	1.13
100	30.76	78.37	26.12	74.81	65.53	1.095
40	22.81	74.9	19.53	74.14	69.28	1.091

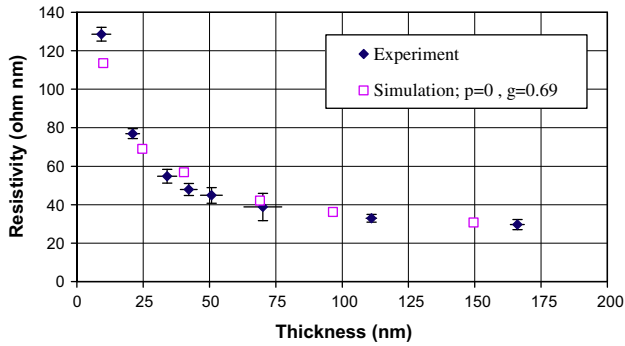


Fig. 4. Experimental resistivity vs. thickness data with the best fit of the simulation. The scattering parameters used in the simulations are $p=0$ and $g=0.69$. The experimental data are from Table 1. Grain size vs. thickness data in Table 2 are used as an input to the simulation.

film thickness (measured with Dektak and presented in Table 2) as inputs to the program. The best overall fit to the experimental data was obtained by adjusting the two parameters used to characterize electron scattering in the film: p is the probability of elastic (specular) scattering from a surface and g is the probability of inelastic scattering by a grain boundary. The best fit is obtained with the $p=0$, $g=0.69$ parameter set. For polycrystalline films it has been observed that the scattering from the surfaces is mostly diffuse; $p \approx 0$ [16,17].

The p parameter of the simulation [2,3] is identical to the “probability of elastic scattering from the surface” parameter of the Fuchs theory [18]. However, the scattering events from the grain boundaries are modeled differently in the simulation [2,3] and in the Mayadas and Shatzkes (MS) theory [19], which is another fundamental theory in the size-effect modeling. The relationship between the grain boundary scattering parameter of the simulation, g , and the quantum mechanical reflection coefficient of the grains, R , of the MS theory was shown to be $g = 0.2617 \ln(R) + 0.9913$ [2]. Therefore, the MS theory correspondent of the best fit is $R = 0.32$. Value of R is a function of the deposition method and conditions. For instance, Wu et al. reported that thermal deposition results in a smaller R parameter than electroplating does [20]. Kuan et al. have reported $R \approx 0.3$ and $p = 0$ for their PVD films, which is similar to what we observed [21].

It is demonstrated in Fig. 5 that Matthiessen’s rule can continue to be used with confidence for films at least as thin as 20 nm. It had been predicted by the simulation program [2] that to use Matthiessen’s rule to calculate the thickness of thinner films (and the cross-section of narrower lines) will lead to increasingly larger underestimates of these dimensions. Looking at Table 1, we cannot argue that this has been verified experimentally, because, although it looks like we have an increasing difference between the Dektak thickness measurements and the thicknesses calculated using Matthiessen’s rule as the films get thinner than 30 nm, the actual difference between the two types of thickness measurements is still within the uncertainty of the Dektak measurements. No correction was made for the consumption of copper due to oxidation in the nominal 150 nm film during the 33 days between the thickness and the sheet resistance measurements of the film. Any reasonable correction, if made, would likely bring the point closer to the zero-difference line in Fig. 5.

4. Conclusion

The size effect on the resistivity of evaporated copper films, ranging in thickness from 9 nm to 167 nm, was determined experimentally from measurements of the electrical sheet resistance and

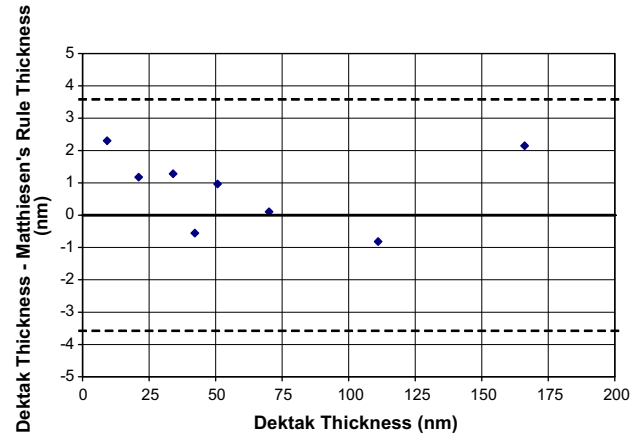


Fig. 5. Difference between thickness obtained with Dektak measurement and Matthiessen’s rule calculation plotted with dashed lines representing the mean standard deviation of the Dektak measurements. (Uncertainties in sheet resistance measurements used in Matthiessen’s rule calculations are negligible in comparison.) The data were taken from Table 1.

the physical thickness. To evaluate a previously published simulation program [2] for studying the size effect in metals, such as copper, the mean grain size was measured for each film thickness, as it is a key input parameter to the program. Good agreement was obtained between the experimental results and the simulated variation of resistivity with film thickness as judged by how well the resistivity versus film thickness curves compared (see Fig. 4). The simulation program is available to others by using the flowcharts and the program code that have been provided [3].

The Electron Back Scatter Diffraction (EBSD) and the X-ray Diffraction (XRD) methods were used, in combination, to determine the mean grain size of the grains in the plane of the film. While the EBSD method is designed to provide such a measure of grain size, which is needed by the simulation program, useful images of the grains could be obtained only for the two thickest films. The XRD method provided data for every film thickness, but it was of the mean thickness of the grains in each film. By using the assumption that the mean grain size in the plane of the film (GS_{xy}) is directly proportional to the mean grain thickness (GS_z) for a given film thickness, the mean grain size in the plane of the film was obtained for all films by using the value for GS_{xy}/GS_z obtained from the thickest film. That such a relationship between the size and thickness of the grains may exist, as was indicated from our observations, could be useful to other researchers in seeing fruitful avenues for further nucleation studies.

Measurements of the change in sheet resistance with temperature for each film thickness were used to calculate the electrical thickness of the films using Matthiessen’s rule. The level of agreement between the physical (Dektak) and the electrical measurements of film thickness over the entire range of film thicknesses showed that Matthiessen’s rule can be used to measure the thickness of copper films as thin as 20 nm. For thinner films, the simulation program predicts significant underestimates of actual film thickness. This prediction could not be evaluated because the differences in the thicknesses noted were less than the uncertainty in the precision of the physical thickness measurements (3–4 nm).

Future work may involve using narrow, patterned features rather than the films used in the present work. Each approach involves tradeoffs: the evaporated film may exhibit different conduction characteristics from a patterned feature; resistivity results from a patterned feature may be dominated by non-uniform cross-section and sidewalls making determination of a unique modeling solution challenging [22]. Recent work by a team including one

of the authors of this paper describes a novel fabrication method to produce patterned copper features with extremely uniform side-walls [23,24].

Acknowledgements

We are pleased to recognize the very helpful assistance of our colleagues at NIST. In particular, we would like to thank James R. Ehrstein for his guidance in the use of the four-point probe measurement of sheet resistance, the generous assistance of Joseph J. Kopanski in using the atomic force microscopy system for characterizing copper films, the discussions with Brian J. Polk in the use of the Dektak profilometer to measure film thickness, the assistance of Monica D. Edelstein with SEM measurements, and the guidance of Gerard Henein and Russell E. Hajdaj at the NIST Center for Nanoscale Science and Technology's Nanofabrication Facility. We also wish to thank David L. Blackburn and Bob R. Keller for many stimulating exchanges during the progress of our work. Finally, we wish to express our appreciation for the work and guidance of Daniel Jossell and the discussions with Thomas P. Moffat during the early attempts to deposit and measure satisfactory thin copper films.

References

- [1] Barnat EV, Nagakura D, Wang P-I, Lu T-M. Real time resistivity measurements during sputter deposition of ultrathin copper films. *JAP* 2002;91(3):1667–72.
- [2] Yarimbiyik AE, Schafft HA, Allen RA, Zaghoul ME, Blackburn DL. Modeling and simulation of resistivity of nanometer scale copper. *Microelectron Reliab* 2006;46(7):1050–7.
- [3] Yarimbiyik AE, Schafft HA, Allen RA, Zaghoul ME, Blackburn DL. Implementation of simulation program for modeling the effective resistivity of nanometer scale film and line interconnects. NIST Internal Report 2006; #7234. <<http://www.eeel.nist.gov/812/nanostructures/NISTIR7234.html>>.
- [4] Schuster CE, Vangel MG, Schafft HA. Improved estimation of the resistivity of pure copper and electrical determination of thin copper film dimensions. *Microelectron Reliab* 2001;41:239–52.
- [5] Smits FM. Measurement of sheet resistivities with the four-point probe. *Bell Syst Tech J* 1958;37:711–8.
- [6] Perloff DS, Gan JN, Wahl FE. Dose accuracy and doping uniformity of ion implant equipment. *Solid State Technol* 1981;24(2):112–20.
- [7] Neter J, Wasserman W, Whitmore GA. *Applied statistics*. 4th ed. Boston, London, Sydney, Toronto: Allyn and Bacon Inc.; 1979.
- [8] <<http://www.ebsd.com>>
- [9] Randle V, Engler O. *Introduction to texture analysis*. Amsterdam: Gordon and Breach Science Publishers; 2000.
- [10] Bartham SF. Crystallite-size determination from line broadening and spotty patterns. In: Kaelble EF, editor. *Handbook of X-rays*. New York: McGraw-Hill; 1967 [chapter 17].
- [11] Warren BE. *X-ray diffraction*. Reading, MA: Addison-Wesley; 1969.
- [12] Bragg L. *The crystalline state*. London: G. Bell & Sons Ltd.; 1949.
- [13] Stafford GR, Vaudin MD, Moffat TP, Armstrong N, Kelley DR. The influence of additives on the room-temperature recrystallization of electrodeposited copper. In: *Third international symposium on electrochemical technology applications in electronics*, 196 Meetings of Electrochemical Society, Honolulu, Hawaii; October 1999.
- [14] Humphreys FJ. Review: grain and subgrain characterization by electron backscatter diffraction. *J Mater Sci* 2001;36:3833–54.
- [15] Keller RR, Geiss RH, Barbosa III N, Sliifka AJ, Read DT. Strain-induced grain growth during rapid thermal cycling of aluminum interconnects. *Metall Mater Trans A* 2007;38A(13):2263–72.
- [16] Sondheimer H. The mean free path of electrons in metals. *Adv Phys* 1952;1(1):1–42.
- [17] Reynolds FW, Stilwell GR. *Phys Rev* 1952;88:418–9.
- [18] Fuchs K. The conductivity of thin metallic films according to the electron theory of metals. *Proc Cambridge Philos Soc* 1938;34:100–8.
- [19] Mayadas AF, Shatzkes M. Electrical-resistivity model for polycrystalline films: the case of arbitrary reflection at external surfaces. *Phys Rev B* 1970;1(4):1382–9.
- [20] Wu W, Brongersma SH, Van Hove M, Maex K. Influence of surface and grain-boundary scattering on the resistivity of copper in reduced dimensions. *Appl Phys Lett* 2004;84(15):2838–40.
- [21] Kuan TS, Inoki CK, Oehrlein GS, Rose K, Zhao Y-P, Wang G-C, et al. Fabrication and performance limits of sub-0.1 micrometer Cu interconnects. *Mat Res Soc Symp Proc* 2000;612(D71):1–8.
- [22] Steinhögl W, Schindler G, Steinlesberger G, Traving M, Engelhardt M. Comprehensive study of the resistivity of copper wires with lateral dimensions of 100 nm and smaller. *J Appl Phys* 2005;97:023706.
- [23] Shulver BJR, Bunting AS, Gundlach AM, Haworth LI, Ross AWS, Smith S, Snell AJ, Stevenson JTM, Walton AJ, Allen RA, Cresswell MW. Extraction of sheet resistance and linewidth from all-copper ECD test structures fabricated from silicon preforms. In: *IEEE international conference on microelectronic test structures*. ICMTS '07; 2007. p. 14–9.
- [24] Shulver BJR, Bunting AS, Gundlach AM, Haworth LI, Ross AWS, Smith S, Snell AJ, Stevenson JTM, Walton AJ, Allen R, Cresswell MW. Extraction of sheet resistance and line width from all-copper ECD test structures fabricated from silicon preforms. *IEEE Transactions on Semiconductor Manufacturing* 2008;21(4):495–503.